

Local density of state fluctuations in 2D superconductor as a probe of quantum diffusion

Mathieu Lizée,^{1,2} Matthias Stosiek,³ Christophe Brun,² Igor Burmistrov,^{4,5} and Tristan Cren²

¹*Laboratoire de Physique de l'École Normale Supérieure, ENS, Université PSL, CNRS, 3 Sorbonne Université, Université Paris Cité, 75005 Paris, France*

²*Institut des Nanosciences de Paris, Sorbonne Universités, UPMC Paris, France*

³*Physics Division, Sophia University, Chiyoda-ku, Tokyo 102-8554, Japan*

⁴*L. D. Landau Institute for Theoretical Physics, acad. Semenova av. 1-a, 142432 Chernogolovka, Russia*

⁵*Laboratory for Condensed Matter Physics, HSE University, 101000 Moscow, Russia*

The interplay of superconductivity and disorder generates a wealth of complex phenomena. In particular, the peculiar structure of diffusive electronic wavefunctions is predicted to increase the superconducting critical temperature in some range of disorder. In this work, we use an epitaxial monolayer of lead showing a simple band structure and homogenous structural disorder as a model system of a 2D superconductor in the weak-antilocalization regime. Then, we perform an extensive study of the emergent fluctuations of local density of states (LDOS) in this material and compare them with both analytical results and numerical solution of the attractive Hubbard model. We show that mesoscopic LDOS fluctuations allow to probe locally both the elastic and inelastic scattering rates which are notoriously difficult to measure in transport measurements.

I. INTRODUCTION

Since the seminal paper by P. W. Anderson, the field of wave localization in disordered media has developed immensely. In the metallic regime, mesoscopic fluctuations of conductance stemming from the diffusion of electrons in a quenched disorder potential have been observed in a wealth of condensed matter systems and are commonly referred to as the ‘weak localization’ signature [1]. A similar signature of weak localization is predicted to emerge in maps of local density of states (LDOS) of 2D metallic systems [2–4] and has already been observed for surface-plasmon modes [5, 6], For electronic modes however, despite several reports of electronic LDOS spatial fluctuations [7–10], theoretical predictions still lack an experimental confirmation.

The interplay of disorder and superconductivity recently shown a renewed experimental (see Refs. [11, 12] for a review) and theoretical interest [13–24] as the pairing of weakly localized ‘multifractal’ electrons was predicted to yield a disorder-enhanced T_c compared to the clean metal case in well chosen conditions [25, 26]. Recently, a first experimental demonstration of a possible multifractal enhancement of T_c in NbSe₂ monolayers has been reported [9]. Although the spatial distribution of the order parameter in this state has recently demonstrated multifractal statistics [27], a clear picture of multifractal superconductivity is still lacking. A deeper understanding of two-dimensional (2D) diffusive superconductors in the multifractal regime is now required to strengthen this discovery and stimulate the engineering of multifractally enhanced superconductors.

In this study, we probe the mesoscopic fluctuations of LDOS in a purely two-dimensional weakly disordered superconductor with high resolution scanning tunneling spectroscopy (STS). In contrast to previous STS studies on thin films [28–33], we prove quantitatively that co-

herent electronic diffusion control the LDOS fluctuations close to the superconducting coherence peak. To generalize our interpretation, we compare our measurements with self-consistent solutions of the attractive Hubbard model on state of the art system size [19, 22]. We demonstrate that the energy dependency of mesoscopic LDOS fluctuations allows to extract both the elastic and inelastic scattering rate of low energy single particle excitations and argue that LDOS spatial fluctuations constitute a valuable toolbox for the study of 2D diffusive systems.

II. EXPERIMENTS

As model systems for the study of 2D weakly disordered electronic systems, epitaxial monolayers of metals on semiconducting surfaces are exceptionally interesting. Firstly, their thickness of the order of the Fermi wavelength along with their good decoupling from the bulk makes them truly two-dimensional. Secondly, they show a wealth of phases with highly uniform and reproducible structural disorder without the need to evaporate chemical contaminants on the sample. Thus, these systems fully fabricated in ultra-high-vacuum are exceptionally clean and homogeneously disordered in contrast with the usually studied substitution alloys [7–9] where the disorder itself already has long range correlations as shown on topographic maps of references [8, 9]. In this work, we focus on the stripped incommensurate (SIC) phase of lead on silicon. The ideal SIC monolayer described in Figure 1a is made of 1.33 monolayer of lead atoms on top of a Si(111) surface. The lead is evaporated on the 7×7 reconstruction of silicon in a home made scanning tunneling microscope. The SIC phase is made of nanometric domains oriented preferentially along 3 directions as shown on large scale in Figures 1c and 1d. The SIC phase has a nanometric mean free path much smaller than the superconducting coherence length $\xi \sim 50$ nm

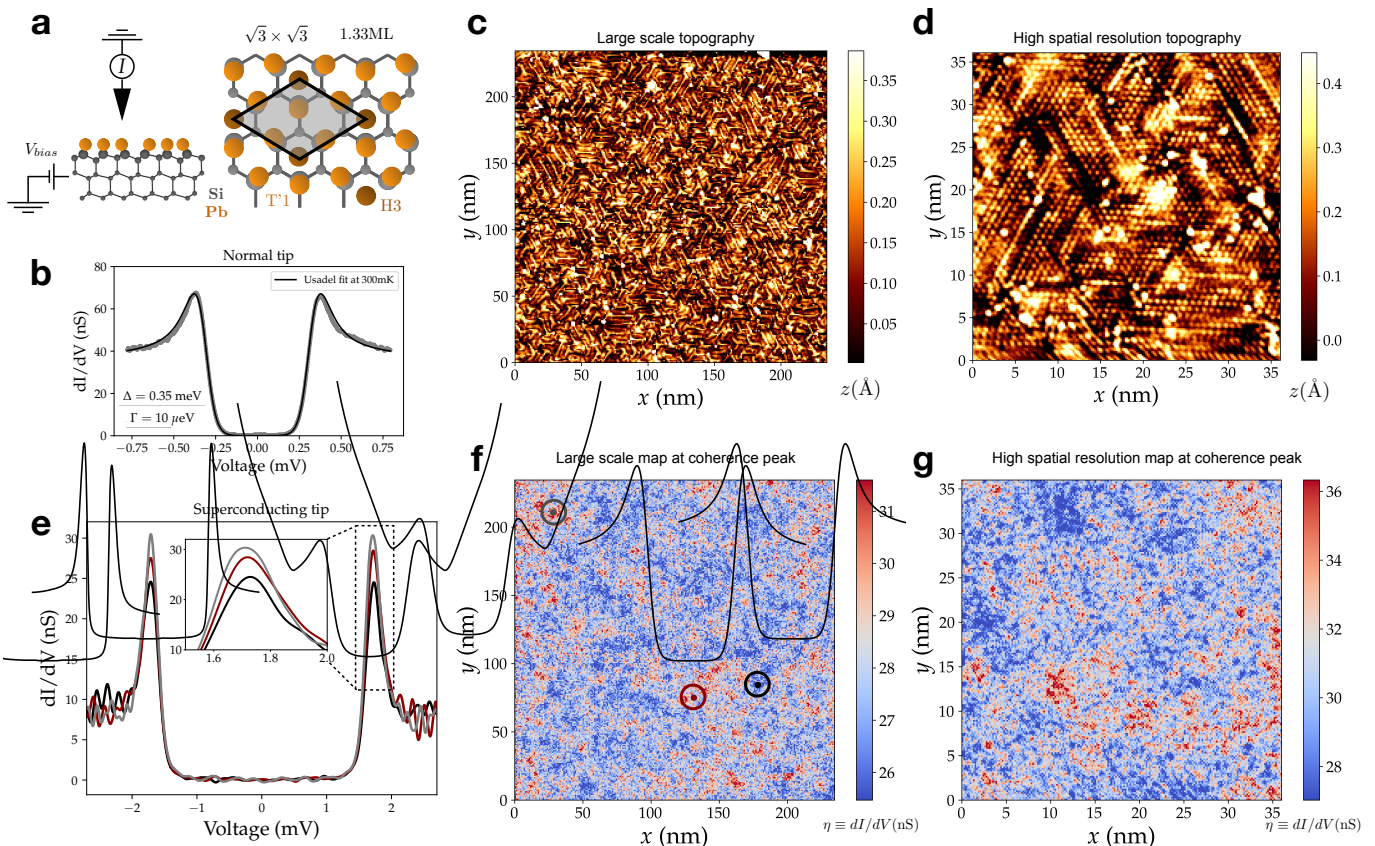


FIG. 1. **Tunneling conductance fluctuations in the stripped incommensurate (SIC) phase of lead on Si** a Description of the scanning tunneling spectroscopy measurement and of the SIC phase (1.33 ML of Pb/Si with $\sqrt{3} \times \sqrt{3}$ symmetry). On **b**, we show the tunneling conductance of the SIC phase measured with a platinum tip along with the best fit with the Usadel formula (see Appendix A). We find $\Delta_{\text{SIC}} = 0.35$ meV and $\Gamma_{\text{SIC}} = 10$ μeV . **c** Topographic image of the SIC monolayer phase. One clearly sees the rotational nanodomains of the $\sqrt{3} \times \sqrt{3}$ phase separated by domain walls made of the $\sqrt{7} \times \sqrt{3}$ reconstruction. An atomically resolved image is shown in **d**. In **e**, several differential conductance spectra (dI/dV) measured at the positions shown on **f** are presented. On **f**, the isoenergy map corresponding to topography **c** at the coherence peak energy $V_{\text{max}} = 1.7$ meV is shown. Symmetrically, on **g**, we show the iso-energy dI/dV map corresponding to topography **d** at the same bias voltage.

[34] making it a prototype system to study 2D diffusive superconductivity at weak disorder. The sample is then cooled to 300 mK, well below its critical temperature of 1.8 K [35]. In Figure 1b, we show the tunneling spectroscopy at 300 mK measured with a platinum tip. The solid line is a solution of the Usadel equation for diffusive superconductors [36] (see Appendix A). The spectrum of Figure 1b was fitted using a gap of $\Delta_{\text{SIC}} = 0.35$ meV and a depairing energy of $\Gamma_{\text{SIC}} = 10$ μeV . In order to probe the mesoscopic fluctuations of this phase, we acquire a large scale (250 nm x 250 nm) spectroscopic map with nanometric spatial resolution. A superconducting tip (bulk lead) is used to increase the energy resolution to 30 μeV [34, 37]. The dI/dV spectrum (Figure 1e) shows sharp coherence peaks at $V_{\text{max}} \sim \Delta_{\text{tip}} + \Delta_{\text{SIC}} = 1.7$ mV. Three individual spectra whose positions are shown in Figure 1f are displayed in Figure 1e.

Displaying the local differential conductance at a given bias voltage V_{bias} yields iso-energy dI/dV maps. On

Figures 1f and 1g, we show the dI/dV map measured at the energy of the coherence peak (1.7 mV) and evidence spatial fluctuations of the differential conductance spanning various scales below the superconducting coherence length $\xi \sim 50$ nm [34, 37]. An interesting feature of this map is indeed that no characteristic scale can be easily identified. This fractal-like behavior is reminiscent of criticality close to the Anderson transition, driven by the cooperation of disorder and electronic coherence. The granular structure observed in topography (see Figures 1c and 1d) does not correlate at all with these ‘emergent’ fluctuations that we consequently attribute to coherent diffusion.

III. ANALYSIS OF FLUCTUATIONS

In order to probe superconducting properties in more details, we focus on LDOS spatial variance close to the

superconducting coherence peak. At voltage V , the variance of iso-energy tunneling conductance maps (shown on Figure 2a for $V \in \{1.5, 1.6, 1.7, 2\}$ mV) writes $\sigma_{\text{exp}}^2(V) = \langle \delta \left(\frac{dI}{dV} \right)^2 \rangle_r$ where to keep notations light, $\eta = dI/dV$ is the experimentally measured differential conductance (see Sec. III C for more accurate definition) and the brackets denote spatial averaging. In Figure 2b, we plot (in green) the variance $\langle \delta \left(\frac{dI}{dV} \right)^2 \rangle$ as a function of bias voltage, showing a maxima close to the coherence peak energy $V_{\text{max}} = E_{\text{max}} + \Delta_{\text{tip}} = 1.7$ mV in agreement with the qualitative observation we made earlier (cf. Figure 1e) that fluctuations are higher at the coherence peak.

A. Theoretical predictions

To rationalize the energy dependency of LDOS spatial variance, we now compute the fluctuations of density of states, $\rho(E, \mathbf{r})$, in a 2D diffusive superconductor. In the following, we sketch a simplified derivation. We have $\rho(E, r) = -\frac{1}{\pi} \text{Im} G^R(E, r, r)$ with $G^R(E, r, r) = \langle r | \frac{1}{E - H + i\eta} | r \rangle$. Like in the mean-field solution to the BCS Hamiltonian, we introduce the Bogoliubov operators and coherence factors $u_\alpha^2/v_\alpha^2 = (1 \pm \epsilon_\alpha / \sqrt{\epsilon_\alpha^2 + \Delta^2})/2$ associated to the single particle eigenstates ϕ_α for the eigenvalue ϵ_α , solutions of the single particle Schrödinger equation including the disordered potential. The LDOS can be written conveniently as:

$$\rho(E, \mathbf{r}) = \sum_{\alpha, s=\pm} \phi_\alpha^2(\mathbf{r}) (1 + \epsilon_\alpha/E) \delta(E - s\sqrt{\epsilon_\alpha^2 + \Delta^2}). \quad (1)$$

$$\langle \delta\rho(E_1, \mathbf{r}_1) \delta\rho(E_2, \mathbf{r}_2) \rangle = \frac{\rho_0^2}{2\pi g} \text{Re} \left\{ \left[1 + X_{E_1} X_{E_2}^* \right] K_0 \left(R \sqrt{\frac{2\gamma_\Phi - iE_1/X_{E_1} + iE_2/X_{E_2}^*}{\hbar D}} \right) - \left[1 - X_{E_1} X_{E_2} \right] K_0 \left(R \sqrt{\frac{2\gamma_\Phi - iE_1/X_{E_1} - iE_2/X_{E_2}}{\hbar D}} \right) \right\}, \quad (4)$$

where $R = |\mathbf{r}_1 - \mathbf{r}_2|$, $K_0(z)$ stands for the modified Bessel function. Also, we introduce $X_E = E/\sqrt{E^2 - \Delta_E^2}$ where we phenomenologically substitute Δ by the complex energy dependent gap-function Δ_E which we estimate using the Usadel model for diffusive superconductors (see Appendix A). Finally, two parameters control the strength of LDOS fluctuations: the dimensionless conductivity $g = \hbar D \rho_0 / 2$ and the effective dephasing rate $\gamma_\Phi = \hbar D / L_\Phi^2$ which we assume to be energy independent. In Figure 3a, we show the energy dependency of the density of states normalized variance $\sigma_\rho^2(E) = \langle \delta\rho(E)^2 \rangle_r / \langle \rho(E) \rangle_r^2$. Here, the conductance is fixed at $g = 30$ and we show the plots for several values of γ_Φ ranging typically between $\Gamma \sim k_B T \sim 30 \mu\text{V}$ and $\Delta \sim 350 \mu\text{V}$. In black, we show the mean density of states spectrum, $\text{Re}(X_E)$, used for this computation, namely the best Usadel fit for the SIC phase (see Ap-

pendix A). We show that σ_ρ^2 has a local minimum close to the coherence peak energy E_{max} , in good agreement with the minimum of normalized variance σ_{exp}^2 at the superconducting coherence peak (Figure 2c). In Figures 3b and 3c, we show that at fixed energy, σ_ρ^2 decreases with increasing conductivity (as expected from the $1/g$ dependency in equation (4)). In Figures 3b and 3d, we demonstrate that increasing dephasing rate γ_Φ – corresponding to smaller system size in a transport experiment (Thouless energy) – reduces the variance σ_ρ^2 . We stress that these dependencies are very natural in the context of mesoscopic fluctuations. Larger electronic phase coherence length and stronger disorder lead to enhanced fluctuations, whether one measures conductance or LDOS fluctuations.

$$F(\epsilon, \omega, \mathbf{r}, \mathbf{r}') \simeq \frac{1}{\pi\omega} \text{Im} \Pi^R(\omega, \mathbf{r}, \mathbf{r}'). \quad (2)$$

In the *diffusive regime at weak disorder*, one gets for the Fourier transform of the polarization operator

$$\Pi^R(\omega, \mathbf{q}) = \rho_0 \frac{Dq^2}{Dq^2 - i\omega}, \quad (3)$$

where D denotes the diffusion coefficient and ρ_0 the density of states of the noninteracting problem at the Fermi level. The full derivation then yields the pair LDOS correlation function at different spatial points $(\mathbf{r}_1, \mathbf{r}_2)$ and different energies (E_1, E_2) [21–23]:

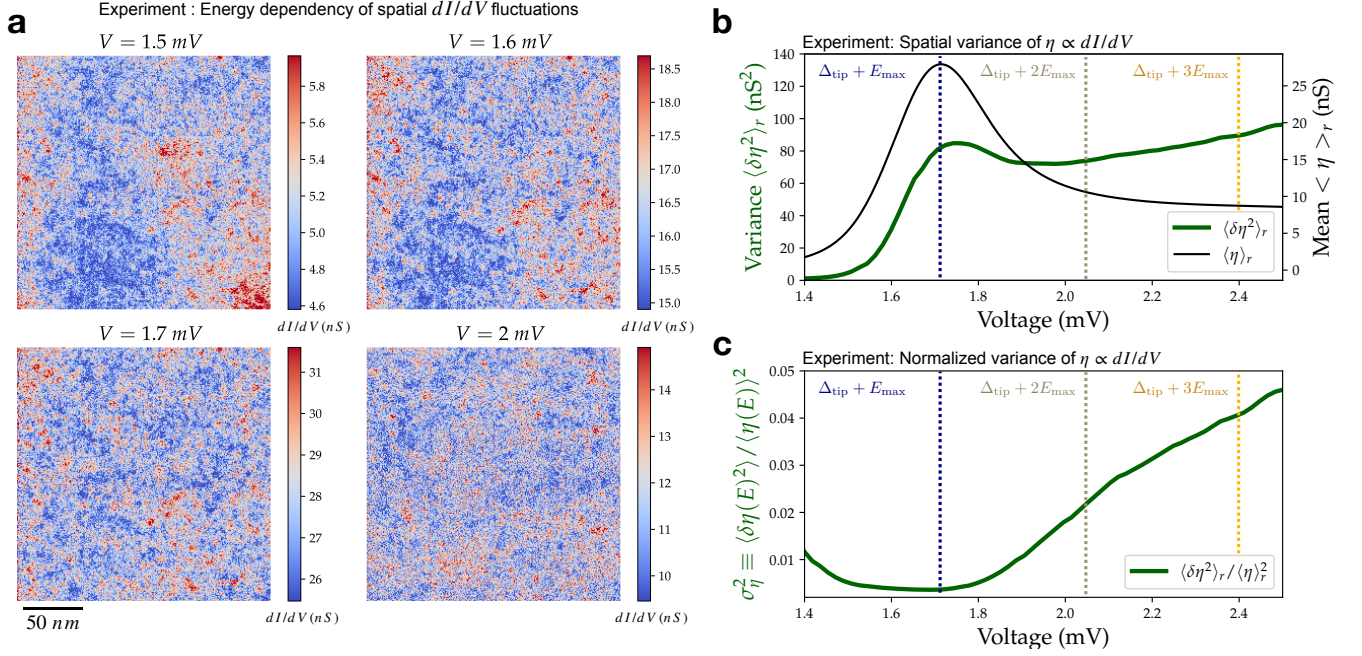


FIG. 2. **Analysis of tunneling conductance fluctuations** **a** Iso-energy maps of the differential conductance $\eta = dI/dV$. **b** Variance (green) and mean value (black) of the tunneling conductance computed on iso-energy maps as a function of the bias voltage. On **c**, we show the bias voltage dependency of the normalized variance $\sigma_{\text{exp}}^2 = \langle \delta\eta(V)^2 \rangle / \langle \eta(V) \rangle^2$ (green).

B. Electronic diffusion in the SIC phase and quantitative extraction of transport parameters

In order to compare the amplitude of LDOS fluctuations with theoretical predictions, we evaluate the diffusion coefficient in the SIC phase by independent means. We refer to previous work by some of the authors where the proximity effect between the SIC phase and small bulky lead islands allowed to estimate the diffusion coefficient of the monolayer [34]. These results are supported by another measurement where the spatial profile of a vortex core allowed us to extract the effective coherence length in the diffusive limit and thus the electronic diffusion coefficient [37]. Both these measurements yield a dirty coherence length $\xi \in [45, 50]$ nm. Writing $\xi = \sqrt{\hbar D / \Delta_{\text{SIC}}}$ with $\Delta_{\text{SIC}} = 0.35$ meV gives a diffusion coefficient $D \in [10, 15]$ cm²/s. We now consider the Einstein relation for the conductivity (per spin orientation) of the monolayer $g = \hbar D \rho_0 / 2$ and using the 2D electron gas model - shown to be appropriate by ARPES measurements [39] - we write for the density of states $\rho_0 = 2 \frac{k_F}{\hbar v_F} = \frac{2m}{2\pi\hbar^2}$ (factor of 2 for the two spin orientations). This leaves us with $g = \frac{mD}{\hbar}$. Using the known effective mass $m = 1.27m_e$ in the SIC phase [35], we can estimate $g \sim 20$. We insist that this value may be underestimated as in the former experiments used to evaluate ξ , the disorder was higher than in the present experiment due to scattering nano-islands not appearing here. Thus we infer that $g = 20$ is in fact a lower bound of the actual conductance and we roughly estimate $g \in [20 - 100]$.

Like we stated earlier, the lead monolayer is weakly disordered and lies deep in the diffusive regime as the mean free path $\ell \sim 1 - 5$ nm much smaller than ξ .

C. Comparison with experiments

We now attempt a quantitative comparison of our theoretical analysis with our experiments on the SIC phase of lead on silicon. Using equation (4), we compute the normalized variance of the tunneling conductance: $\sigma_\eta^2 = \langle \delta\eta(V)^2 \rangle_r / \langle \eta(V) \rangle_r^2$ at a bias voltage V . Here, we take into account the tip density of states and variations of the tip height above the sample during the measurement. All details are given in Appendix B. The formula we obtain for σ_η^2 (Eq. (B5)) is a straightforward energy integration of the density of states correlator given in equation (4).

The tunneling conductance variance can then be compared to the experimentally measured σ_{exp}^2 (in green) on Figure 3e. The thin lines are semi-analytical calculations of σ_η for $g \in \{20, 30, 50, 100\}$ from Eq. (B5). For each value of g , we plot the theoretical curve for a few dephasing rates γ_Φ which best reproduce the experimental variance. We stress that no free parameter is used here as g takes very reasonable values for the SIC phase [34, 37] while the dephasing rate γ_Φ is constrained in a rather narrow window of physically relevant energies $\gamma_\Phi \in [1, 150]$ $\mu\text{eV} \sim [k_B T / 30, \Delta_{\text{SIC}} / 2]$. We obtain an excellent quantitative agreement between experiment and theoretical predictions for a range of parameters corre-

Theory for LDOS spatial fluctuations

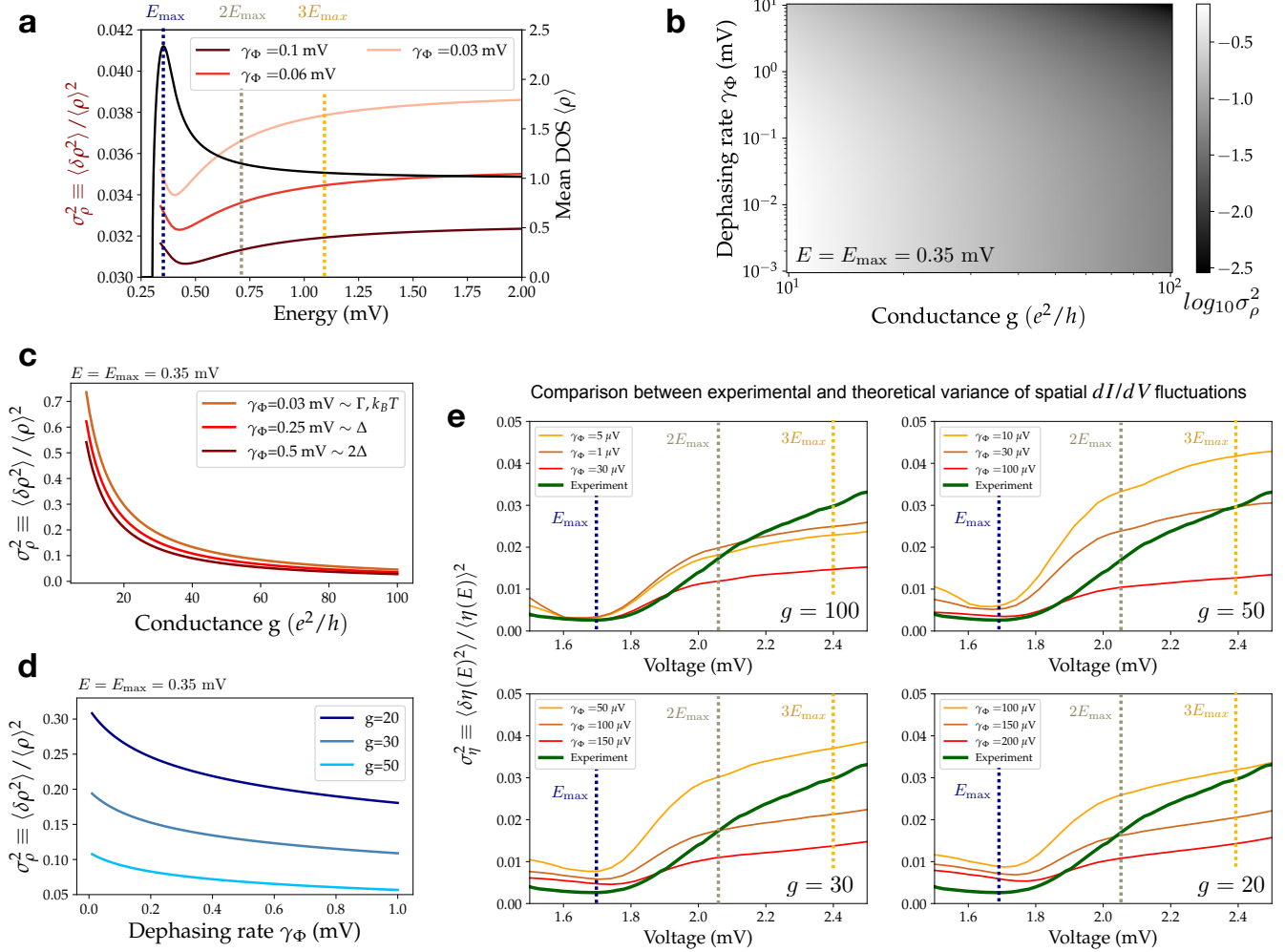


FIG. 3. **Analysis of tunneling conductance fluctuations** On panels **a-d**, we describe the fluctuations of density of states computed semi-analytically as a function of energy E , conductance g and effective dephasing rate γ_Φ . On **a**, we show the energy dependency of the normalized variance σ_ρ^2 (red) at $g = 30$ and several values of $\gamma_\Phi \in \{0.03, 0.06, 0.1\}$ mV. In black, we show the mean density of states used for the calculation (solution of Usadel equation, *cf.* Appendix A). On **b-d**, we now fix the energy at $E_{\max} = 0.35$ mV and plot on **b** a color-map the log of σ_ρ^2 as a function of both conductance and dephasing rate. On **c**, we show the dependency of σ_ρ^2 on conductance for $\gamma_\Phi \in \{0.03, 0.25, 0.5\}$ mV. On **d**, we show the dependency on dephasing rate for $g \in \{20, 30, 50\}$. On **e**, we compare the experimentally measured normalized variance of tunneling conductance σ_η^2 with the one computed semi-analytically from density of states correlations (Eq.(B5) derived in Appendix B from Eq.(4)). We plot the theoretical prediction for $g \in \{20, 30, 50, 100\}$ and the levels of dephasing which best reproduce the experimental data in each case. We stress that no free parameter is used here.

sponding to $g \in [50, 100]$ where the energy dependency of the normalized variance close to the coherence peak is very nicely reproduced.

Thus, we claim that emergent dI/dV spatial fluctuations in the 2D superconductor are a direct probe of coherent diffusion, well reproduced by a simple analytical model (section III A). Although a quantitative extraction of γ_Φ is difficult in our case, our results show that scanning tunneling spectroscopy intrinsically allows for a local measurement of both dimensionless conductance and electronic coherence length. This non invasive local probe explores structurally optimized regions

far from step edges or contacts. This direct probe of electronic diffusion, should be considered as complementary to transport measurements. Moreover, it shows a huge - yet almost unexplored - potential for improvement through the detailed analysis of spatial correlations and in particular of the spatial structure of wavefunctions which is expected to be the very cause of multifractal T_c enhancement.

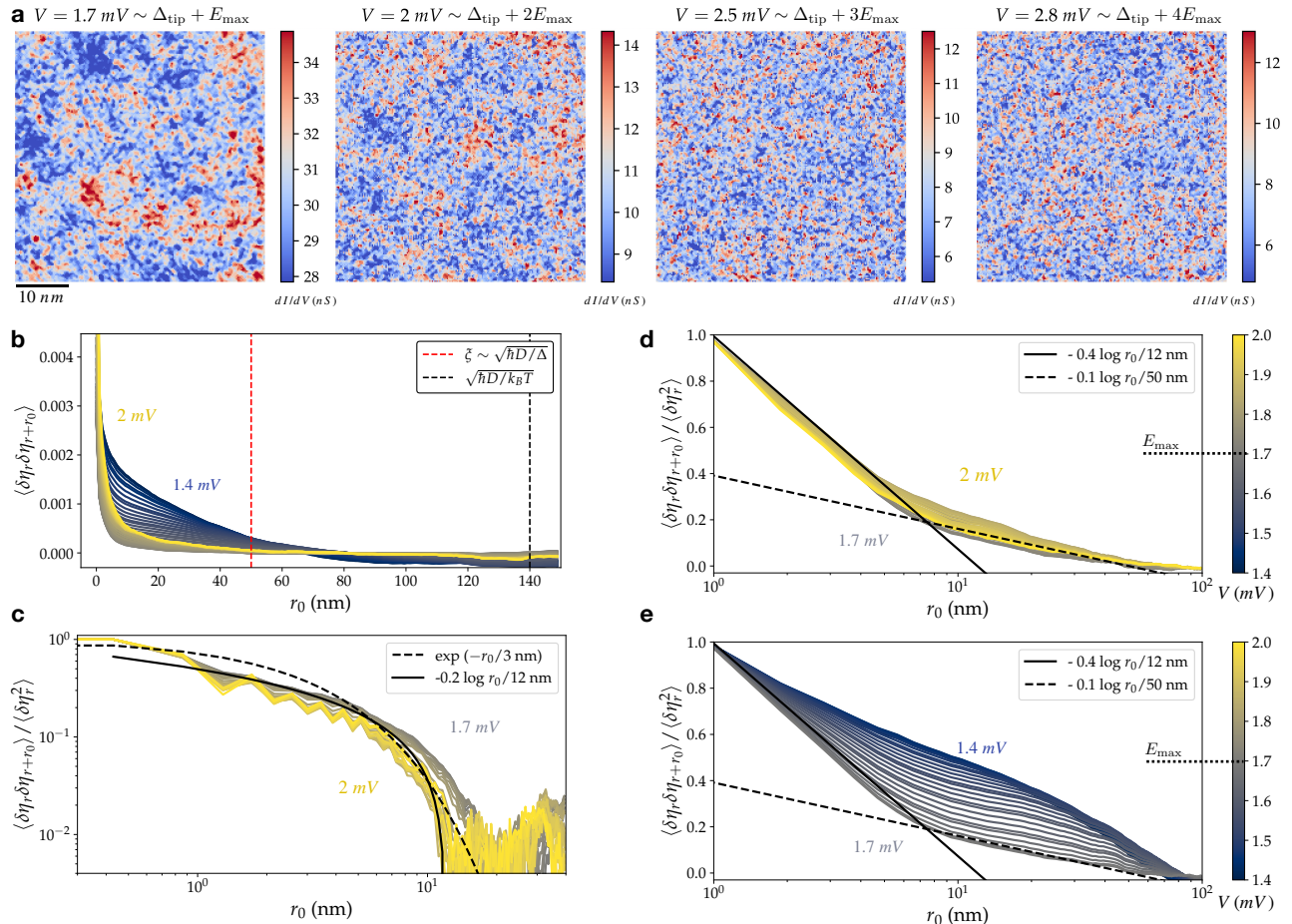


FIG. 4. **dI/dV spatial correlations** On **a**, we show several iso-energy high resolution differential conductance maps for $E = V - \Delta_{\text{tip}} \in \{1, 2, 3, 4\} E_{\text{max}}$. On panel **b**, we show the angle averaged 2-point correlations on large scale maps as a function of distance and bias voltage (color scale for panels **b-e** given on panels **d,e**). On this plot, we also show the position of superconducting coherence length ξ (red) and the diffusion length corresponding to energy scale $k_B T \sim 30 \mu\text{eV}$ (black). On **c**, we plot the angle averaged auto-correlation computed on small scale maps. On **d,e**, we use lin-log scales to evidence the peculiar behavior of the auto-correlation (normalized by its zero distance value). On **d**, we focus on energies below E_{max} and on **e**, on energies above E_{max} .

IV. SPATIAL CORRELATIONS

After considering the variance of the iso-energy maps and thus disregarding the spatial structure of dI/dV fluctuations, we briefly focus on the analysis of spatial correlations of the local conductance: $\langle \delta\eta_r \delta\eta_{r+r_0} \rangle$. On Figure 4a, we show several high resolution conductance maps at various energies above the coherence peak $E = V - \Delta_{\text{tip}} \in \{0.35, 0.7, 1.2, 1.5\} \text{ mV} \sim \{1, 2, 3, 4\} E_{\text{max}}$. We observe very clearly that large scale spatial structures at E_{max} tend to disappear with increasing energy.

To explore the iso-energy spatial correlations of tunneling conductance, we plot on Figure 4b the angle-averaged 2-point correlation function as a function of distance r_0 . The color of the curve represents the energy at which

it is measured. On Figure 4c, we use a log-log representation of the auto-correlation function on high resolution maps (normalized by its value at 0.1 nm). To better show the angle averaged radial decay at various energies on large scale 250 nm maps, we normalize the auto-correlation by its value at $r_0 = 1 \text{ nm}$ and plot them for energies below E_{max} on Figure 3d and above E_{max} on Figure 3e where the curve's color is coding its energy below 1.4 and 2 mV. It is apparent here that above E_{max} , these auto-correlation profiles depend only very weakly on energy. On Figure 4e, we show that the spatial auto-correlation function has a short range regime with steep decay up to approximately 10 nm followed by a long range regime with a slower decay. As made visible with the black lines, two apparently log-decay regimes

are identified with characteristic distance slopes of 12 and 50 nm for the short and long range regimes respectively. Although they are not true correlation lengths, these two characteristic lengths in the auto-correlation function seem very natural as 10 nm correspond to the typical nanocrystal size of the SIC monolayer and 50 nm to its superconducting coherence length.

To deepen our understanding of these LDOS fluctuations, we complement our experimental work with a numerical study of a superconducting electrons on a 2D disordered lattice in the weak disorder regime. The deep similarity between experimental and our fully self-consistent tight-binding models then allow us to make very precise comparison between the numerical, experimental and analytical studies.

V. NUMERICAL STUDY OF LDOS FLUCTUATIONS WITH THE ATTRACTIVE HUBBARD MODEL

We write and solve a tight-binding model tailored to match the experimental system: a weakly disordered 2D diffusive superconductor of comparable conductivity and dephasing rates. We consider the attractive- U Hubbard model on the square lattice in two-dimensions with double-periodic boundary conditions. Within the mean-field approximation the Hamiltonian reads ($U > 0$)

$$\hat{H} = -t \sum_{\langle i,j \rangle, \sigma} \hat{c}_{i,\sigma}^\dagger \hat{c}_{j,\sigma} + \sum_{i,\sigma} (V_i - \mu - U n(\mathbf{r}_i)/2) \hat{n}_{i,\sigma} + \sum_i \Delta(\mathbf{r}_i) \hat{c}_{i,\uparrow} \hat{c}_{i,\downarrow} + \text{h.c.} \quad (5)$$

where $\hat{c}_{j,\sigma}^\dagger$ and $\hat{c}_{j,\sigma}$ denote the creation and annihilation operators of an electron with spin $\sigma = \pm 1/2$ on site j . The on-site disorder potential is drawn from a box distribution, $V_i \in [-W, W]$ with a disorder strength fixed at $W=0.5$ in an attempt to match the experimental disorder strength. The chemical potential μ fixes the filling factor to 0.3. Throughout this work the interaction is taken as $U = 2.2t$ and the system size as $L = 192$, the local occupation number $n(\mathbf{r}_i)$ and the pairing amplitude $\Delta(\mathbf{r}_i)$ are determined self-consistently,

$$n(\mathbf{r}_i) = \sum_{\sigma} \langle \hat{n}_{i,\sigma} \rangle, \quad \Delta(\mathbf{r}_i) = U \langle \hat{c}_{i,\downarrow}^\dagger \hat{c}_{i,\uparrow}^\dagger \rangle, \quad (6)$$

where $\hat{n}_{i,\sigma} = \hat{c}_{i,\sigma}^\dagger \hat{c}_{i,\sigma}$. We solve Eqs. (5)–(6) iteratively until a self-consistent solution is obtained (see Ref. [19] for further computational details). The ensemble averaging involves typically more than a hundred samples and the density of states is computed by averaging on an energy scale $\langle \Delta \rangle / 10$ in good matching with the experimental situation ($\Gamma_{\text{tip}} = 20 \mu\text{eV} \sim \Delta_{\text{SIC}}/10$).

On Figure 5, we show the results of the numerical investigation and compare them with both the analytical theory derived earlier and the experimental results. We

check that, as expected at weak disorder [21, 23] and in agreement with the experiment, Δ shows very small fluctuations. On panels 5a and 5b, we show local density of state maps taken at $E = E_{\text{max}}$ and $E = 2E_{\text{max}}$. In excellent agreement with the experimental results (Figure 4), a strong qualitative difference is observed on the maps: fluctuations show much longer range correlations close to E_{max} than at higher energy.

A. Normalized variance

Like in the experimental section above, we now proceed to study the normalized variance of the LDOS spatial fluctuations. On Figure 5c, we show the mean density of states of the numerical model (black line) along with the normalized variance σ^2 (red). We compare the numerically obtained LDOS variance with the analytical prediction derived from Eq. (4) depending on dimensionless conductance g and dephasing rate γ_Φ . As our tight binding approach considers solutions of the stationary Schrödinger equation, it does not include dephasing. γ_Φ is thus substituted by a Thouless energy corresponding to diffusive motion at the scale of system size: $\gamma_\Phi = \frac{\hbar D}{L^2}$. Knowing the density of states and Fermi velocity of the 2D electron gas, we manage to compute Eq.(4) as a function of a single parameter, the dimensionless conductance g (with $\gamma_\Phi = g t a^2 / L^2$). We find that $g \sim 10$ reproduce almost perfectly the numerical results (red) on all the energy range we considered. Overall, we show that our theoretical analysis, parametrized by g and γ_Φ bridges very well the experimental measurements with the tight-binding model and rationalizes quantitatively the energy-dependent normalized LDOS variance.

B. LDOS distributions

We already know from several experiments that disordered systems tend to yield log-normal LDOS distributions [7, 8]. More precisely, close to Anderson transition, a log-normal distribution of the LDOS is expected [4, 16, 21, 22]. Here, we study the distribution function of both our experimental dI/dV maps and the ones obtained from the attractive Hubbard model. Starting with the numerical results, we plot on Figure 5d, the distribution of the LDOS distribution at fixed energy along with the corresponding (i.e. of same variance) Gaussian and log-normal laws (see Appendix C). A clear log-normal behavior is identified on all the energy range between E_{max} and $3E_{\text{max}}$ as confirmed on panel 5e which compares the root-mean-squared (RMS) deviation of the distribution to either the Gaussian or the log-normal model. Turning to the experimental data, we show on Figure 5f, the dI/dV distribution with Gaussian (dotted line) and log-normal laws (solid line) of same variance at voltage corresponding to E_{max} and $1.5E_{\text{max}}$. Like before, we plot on panel 5h the RMS deviation to the Gaussian or

log-normal model. The log-normal model being more accurate is a hint of the multifractal nature of the LDOS fluctuations close to the superconducting coherence peak.

CONCLUSION

As a model system for two-dimensional weakly disordered superconductor where multifractal superconductivity is being actively pursued, we prepared a single layer of lead on silicon where electrons are anti-localized in a controlled crystalline disorder and become superconducting below 1.8 K. We report the measurement of tunneling conductance fluctuations with exquisite spatial and spectral resolutions on scales exceeding the superconducting coherence length. To our knowledge, this study is the first to link experimentally spatial LDOS fluctuations with weak anti-localization physics. To support our analysis, we used the attractive Hubbard model with a disorder level finely tuned to match the experiment and probed LDOS fluctuations close to the superconducting coherence peak. Both experimental and numerical results are shown to be consistent with the mesoscopic fluctuations physics in the weakly anti-localized regime usually probed through transport measurements. The LDOS fluctuation's amplitude depends on two parameters which can be probed and quantitatively extracted in this way: the metal's conductance and an effective electronic dephasing rate.

ACKNOWLEDGMENTS

The work of I.S.B. was funded in part by the Russian Ministry of Science and Higher Educations, the Basic Re-

search Program of HSE, and by the Russian Foundation for Basic Research, grant No. 20-52-12013.

Appendix A: Mean density of state

We use the Usadel model [36, 40] to describe the diffusive SIC phase as the mean free path is much smaller than the superconducting coherence length in this sample: $\ell \sim 1 \text{ nm} \ll \xi \sim 50 \text{ nm}$. In more details, we use the spectral angle θ_E parametrisation, with θ_E a solution of an homogenous Usadel equation with a depairing term Γ :

$$iE \sin(\theta_E) + \Delta \cos(\theta_E) - \Gamma \sin(\theta_E) \cos(\theta_E) = 0 \quad (\text{A1})$$

The solution of this equation θ_E yields $X_E = \frac{E}{\sqrt{E^2 - \Delta^2}} = \cos(\theta_E)$ from which the density of states $\text{Re}(X_E)$ is obtained.

Using Eq. (A2) and Eq. (A1), we convolve the density of states of the tip with the one of the sample (along with the Fermi distribution at 300 mK) in order to reproduce the mean differential conductance.

$$I \propto \int \rho_{\text{tip}}(E - eV) \rho_{\text{SIC}}(E, \mathbf{r}) (f(E) - f(E - eV)) dE \quad (\text{A2})$$

where ρ_{tip} and ρ_{SIC} are the respective energy-dependent DOS of the tip and the SIC phase. As detailed on Figure 6, we find that the lead tip is very well described by a Usadel superconductor ($\Delta_{\text{tip}} = 1.345 \text{ meV}$, $\Gamma_{\text{tip}} = 20 \mu\text{eV}$). The SIC phase is found to be very well described by $\Delta_{\text{SIC}} = 0.35 \text{ meV}$ and $\Gamma_{\text{SIC}} = 10 \mu\text{eV}$ in excellent agreement with additional measurements using a normal tip (Figure 1b and 6a) and with earlier works [34, 37].

Appendix B: Differential conductance variance computation

We now attempt to rationalise the tunneling conductance spatial fluctuations. Considering a simplified expression for the tunneling current, we write it as a zero temperature convolution of tip and sample density of states Eq.(A2). Experimentally, the tip's height above the sample and thus the transmission's coefficient t is not constant but rather controlled by fixing the high voltage current $I(V_\Lambda = 3 \text{ mV})$ to 2 nA. Trying to estimate density of state leads us to compute:

$$\eta(V, \mathbf{r}) = \frac{\overline{I(V_\Lambda)}}{I(V_\Lambda, \mathbf{r})} \frac{\partial I}{\partial V}(V, \mathbf{r}) \quad (\text{B1})$$

At $T = 0$, we write for the tunneling current I and the tunneling conductance dI/dV :

$$I = |t|^2 \int_0^V dE \rho_{\text{tip}}(E - eV) \rho(E, \mathbf{r}) \quad \text{and} \quad \frac{\partial I}{\partial V} = |t|^2 \rho_{\text{tip}}(0) \rho(V, \mathbf{r}) - |t|^2 \int_0^V dE \rho'_{\text{tip}}(E - V) \rho(E, \mathbf{r}) \quad (\text{B2})$$

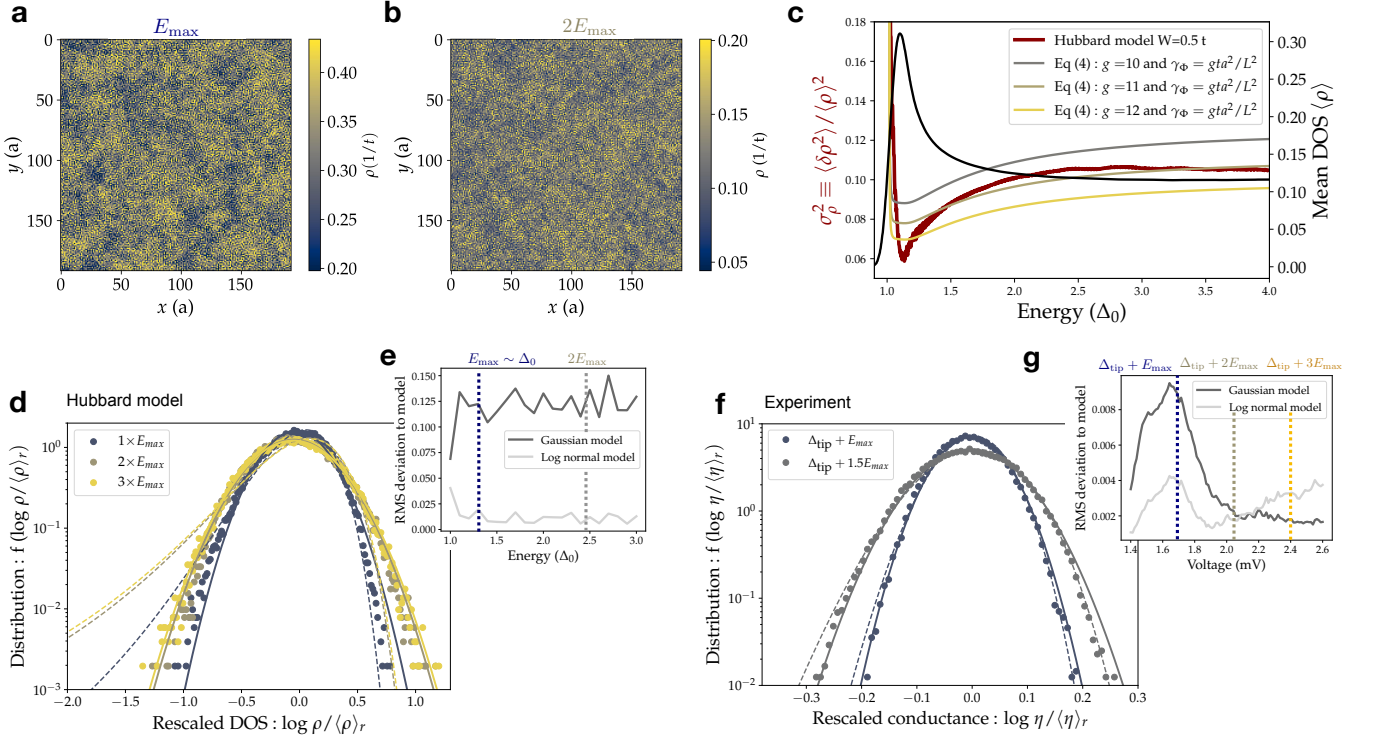


FIG. 5. **Disordered attractive Hubbard model and LDOS distributions** On panel **a,b**, we show local density of state maps taken at $E = E_{\max}$ and $2E_{\max}$ using the attractive Hubbard model. The density of states is given in units of $1/t$ with t the hopping energy. On panel **c**, we show the mean density of states of the numerical model (black line) along with the normalized variance σ^2 (red). We plot analytical prediction from Eq. (4) for $g \in \{10, 11, 12\}$. We stress that no free parameter has been optimized. On panel **d**, we plot the LDOS distribution at fixed energy along with the corresponding gaussian (dotted line) and log-normal (solid line) distributions (*ie*: of same variance). Distribution functions are given in Appendix C. On panel **e**, we show the RMS deviation to respectively gaussian (dark grey) and log normal (light grey) models. Panels **f,g** are analogous to **d,e** for the experimental dI/dV distribution.

where $\rho'_{\text{tip}}(E) \equiv d\rho_{\text{tip}}(E)/dE$. It is convenient to introduce the following notations

$$\bar{j}(V) = \int_0^V dE \rho_{\text{tip}}(E - V) \bar{\rho}(E) \quad \text{and} \quad \bar{j}'(V) = \rho_{\text{tip}}(0) \bar{\rho}(V) - \int_0^V dE \rho'_{\text{tip}}(E - V) \bar{\rho}(E). \quad (\text{B3})$$

Assuming that fluctuations $\delta\rho(E, \mathbf{r}) = \rho(E, \mathbf{r}) - \bar{\rho}(E)$ near the average DOS $\bar{\rho}(E)$ are weak, we find:

$$\frac{\delta\eta(V, \mathbf{r})}{I(V_\Lambda)} = \frac{\rho_{\text{tip}}(0) \delta\rho(V, \mathbf{r})}{\bar{j}(V_\Lambda)} - \int_0^\infty dE \delta\rho(E, \mathbf{r}) \frac{\rho'_{\text{tip}}(E - V) \bar{j}(V_\Lambda) \Theta(V - E) + \rho_{\text{tip}}(E - V_\Lambda) \bar{j}'(V) \Theta(V_\Lambda - E)}{[\bar{j}(V_\Lambda)]^2}. \quad (\text{B4})$$

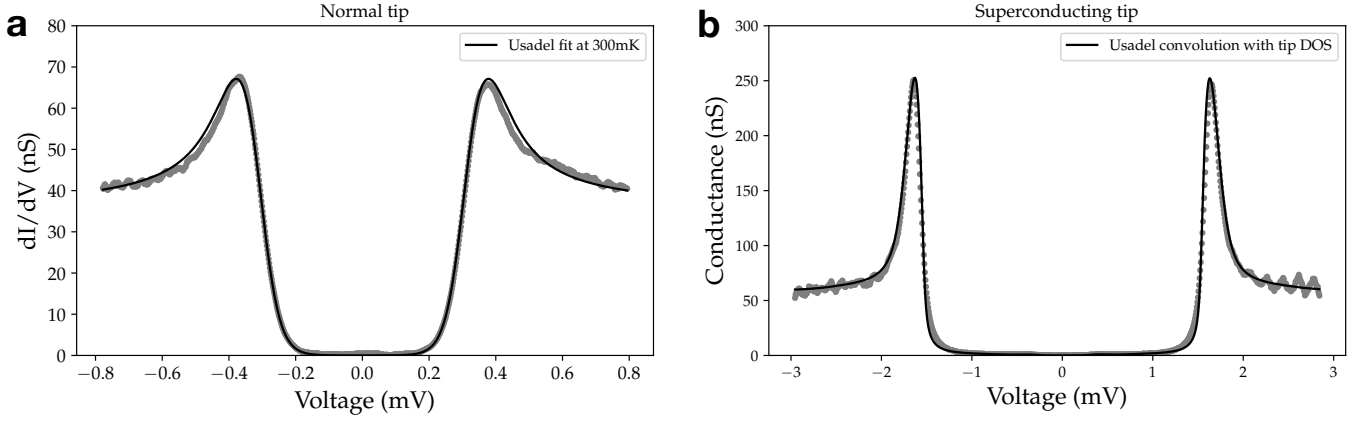


FIG. 6. **Fit of the mean conductance** On **a**, the mean differential conductance measured with a platinum tip is shown as a function of the bias voltage along with the best Usadel fit. On panels **b**, we show the mean dI/dV curve of the large scale spectroscopic map measured with a bulk lead tip while the solid line is a convolution of the Usadel density of states for the sample with the tip density of states at finite temperature.

Here $\Theta(x) = 1$, for $x > 0$ and zero otherwise. Hence we obtain

$$\begin{aligned}
\frac{\langle \delta\eta(V_1, \mathbf{r}_1) \delta\eta(V_2, \mathbf{r}_2) \rangle}{[I(V_\Lambda)]^2} &= \frac{\rho_{\text{tip}}^2(0)}{\bar{j}(V_\Lambda)\bar{j}'(V_\Lambda)} \langle \delta\rho(V_1, \mathbf{r}_1) \delta\rho(V_2, \mathbf{r}_2) \rangle \\
&- \frac{\rho_{\text{tip}}(0)}{\bar{j}(V_\Lambda)} \int_0^\infty dE \langle \delta\rho(V_1, \mathbf{r}_1) \delta\rho(E, \mathbf{r}_2) \rangle \frac{\rho'_{\text{tip}}(E - V_2) \bar{j}(V_\Lambda) \Theta(V_2 - E) + \rho_{\text{tip}}(E - V_\Lambda) \bar{j}'(V_2) \Theta(V_\Lambda - E)}{[\bar{j}(V_\Lambda)]^2} \\
&- \frac{\rho_{\text{tip}}(0)}{\bar{j}(V_\Lambda)} \int_0^\infty dE \langle \delta\rho(V_2, \mathbf{r}_2) \delta\rho(E, \mathbf{r}_1) \rangle \frac{\rho'_{\text{tip}}(E - V_1) \bar{j}(V_\Lambda) \Theta(V_1 - E) + \rho_{\text{tip}}(E - V_\Lambda) \bar{j}'(V_1) \Theta(V_\Lambda - E)}{[\bar{j}(V_\Lambda)]^2} \\
&+ \int_0^\infty dE_1 \int_0^\infty dE_2 \langle \delta\rho(E_1, \mathbf{r}_1) \delta\rho(E_2, \mathbf{r}_2) \rangle \frac{\rho'_{\text{tip}}(E_1 - V_1) \bar{j}(V_\Lambda) \Theta(V_1 - E_1) + \rho_{\text{tip}}(E_1 - V_\Lambda) \bar{j}'(V_1) \Theta(V_\Lambda - E_1)}{[\bar{j}(V_\Lambda)]^2} \\
&\times \frac{\rho'_{\text{tip}}(E_2 - V_2) \bar{j}(V_\Lambda) \Theta(V_2 - E_2) + \rho_{\text{tip}}(E_2 - V_\Lambda) \bar{j}'(V_2) \Theta(V_\Lambda - E_2)}{[\bar{j}(V_\Lambda)]^2}. \tag{B5}
\end{aligned}$$

Appendix C: Iso-energy LDOS distribution

We compare the iso-energy dI/dV distributions to either Gaussian or log-normal models of variance σ . The distribution of the logarithm of normalized density of states $x = \log(\rho(E, r)/\langle \rho(E, r) \rangle_r)$ writes for a Gaussian distribution:

$$f_{\text{log-n}}(x) = \frac{1}{\sqrt{2\pi\sigma^2}} \exp\left[x - \frac{(e^x - 1)^2}{2\sigma^2}\right] \tag{C1}$$

For a log normal distribution which is expected by the theoretical analysis and recovered in the numerical work, the log of the normalized LDOS x is distributed following:

$$f_n(x) = \frac{1}{\sqrt{2\pi\sigma^2}} \exp\left[-\frac{(x + \sigma^2/2)^2}{2\sigma^2}\right] \tag{C2}$$

[1] E. Akkermans and G. Montambaux, *Mesoscopic Physics of Electrons and Photons* (2007).

[2] F. Wegner, *Z. Phys. B* **36**, 209.

- [3] C. Castellani and L. Pelitit, *J. Phys. A* **19**, L429 (1986).
- [4] I. V. Lerner, *Phys. Lett. A* **133**, 253 (1988).
- [5] R. Carminati, A. Cazé, D. Cao, F. Peragut, V. Krachmalnicoff, R. Pierrat, and Y. De Wilde, **70**, 1.
- [6] V. Krachmalnicoff, E. Castanié, Y. De Wilde, and R. Carminati, **105**, 183901.
- [7] A. Richardella, P. Roushan, S. Mack, B. Zhou, D. A. Huse, D. D. Awschalom, and A. Yazdani, *Science* **327**, 665.
- [8] B. Jäck, F. Zinser, E. J. König, S. N. P. Wissing, A. B. Schmidt, M. Donath, K. Kern, and C. R. Ast, *Physical Review Research* **3**, 013022.
- [9] K. Zhao, H. Lin, X. Xiao, W. Huang, W. Yao, M. Yan, Y. Xing, Q. Zhang, Z.-X. Li, S. Hoshino, J. Wang, S. Zhou, L. Gu, M. S. Bahramy, H. Yao, N. Nagaosa, Q.-K. Xue, K. T. Law, X. Chen, and S.-H. Ji, *Nature Physics* **15**, 904.
- [10] M. Morgenstern, J. Klijn, C. Meyer, and R. Wiesendanger, **90**, 056804.
- [11] V. F. Gantmakher and V. T. Dolgopolo, [arXiv:1004.3761](https://arxiv.org/abs/1004.3761) [*cond-mat*] 1004.3761.
- [12] B. Sacépé, M. Feigel'man, and T. M. Klapwijk, *Nat. Phys.* **16**, 13 (2020).
- [13] M. Feigel'man, L. Ioffe, V. Kravtsov, and E. Cuevas, *Annals of Physics* **325**, 1390.
- [14] L. Dell'Anna, *Phys. Rev. B* **88**, 195139 (2013).
- [15] I. S. Burmistrov, I. V. Gornyi, and A. D. Mirlin, *Physical Review B* **92**, 014506 ().
- [16] I. S. Burmistrov, I. V. Gornyi, and A. D. Mirlin, *Physical Review B* **93**, 205432 (), 1603.03017.
- [17] M. N. Gastiasoro and B. M. Andresen, *Phys. Rev. B* **98**, 184510 (2018).
- [18] B. Fan and A. M. García-García, *Phys. Rev. B* **101**, 104509 (2020).
- [19] M. Stosiek, B. Lang, and F. Evers, *Physical Review B* **101**, 144503 ().
- [20] B. Fan and A. M. García-García, *Phys. Rev. B* **102**, 184507 (2020).
- [21] I. S. Burmistrov, I. V. Gornyi, and A. D. Mirlin, [arXiv:2101.12713](https://arxiv.org/abs/2101.12713) [*cond-mat*] (), 2101.12713.
- [22] M. Stosiek, F. Evers, and I. S. Burmistrov, [arXiv:2107.06728](https://arxiv.org/abs/2107.06728) [*cond-mat*] (), 2107.06728.
- [23] E. S. Andriyakhina and I. S. Burmistrov, *JETP* **135**, 484 (2022).
- [24] X. Zhang and M. S. Foster, *Phys. Rev. B* **106**, L180503 (2022).
- [25] M. V. Feigel'man, L. B. Ioffe, V. E. Kravtsov, and E. A. Yuzbashyan, *Phys. Rev. Lett.* **98**, 027001 (2007).
- [26] I. S. Burmistrov, I. V. Gornyi, and A. D. Mirlin, *Physical Review Letters* **108**, 017002 ().
- [27] C. Rubio-Verdú, A. M. García-García, H. Ryu, J. Zaldívar, S. Tang, B. Fan, Z.-X. Shen, K. Mo, J. I. Pascual, and M. M. Ugeda, , 34.
- [28] B. Sacepe, C. Chapelier, T. I. Baturina, V. M. Vinokur, M. R. Baklanov, and M. Sanquer, *Phys. Rev. Lett.* **101**, 157006 (2008).
- [29] M. Mondal, A. Kamlapure, M. Chand, G. Saraswat, S. Kumar, J. Jesudasan, L. Benfatto, V. Tripathi, and P. Raychaudhuri, *Phys. Rev. Lett.* **106**, 047001 (2011).
- [30] Y. Noat, V. Cherkez, C. Brun, T. Cren, C. Carillet, F. Debontridder, K. Ilin, M. Siegel, A. Semenov, H.-W. Hübers, and D. Roditchev, *Phys. Rev. B* **88**, 014503 (2013).
- [31] D. Sherman, B. Gorshunov, S. Poran, N. Trivedi, E. Farber, M. Dressel, and A. Frydman, *Phys. Rev. B* **89**, 035149 (2014).
- [32] B. Sacépé, C. Chapelier, T. I. Baturina, V. M. Vinokur, M. R. Baklanov, and M. Sanquer, *Nature Communications* **1**, 140 ().
- [33] B. Sacépé, T. Dubouchet, C. Chapelier, M. Sanquer, M. Ovadia, D. Shahar, M. Feigel'man, and L. Ioffe, *Nature Physics* **7**, 239 ().
- [34] V. Cherkez, J. Cuevas, C. Brun, T. Cren, G. Ménard, F. Debontridder, V. Stolyarov, and D. Roditchev, *Physical Review X* **4**, 011033.
- [35] C. Brun, T. Cren, and D. Roditchev, *Superconductor Science and Technology* **30**, 013003 ().
- [36] K. D. Usadel, **25**, 507.
- [37] C. Brun, T. Cren, V. Cherkez, F. Debontridder, S. Pons, D. Fokin, M. C. Tringides, S. Bozhko, L. B. Ioffe, B. L. Altshuler, and D. Roditchev, *Nature Physics* **10**, 444 ().
- [38] P. A. Lee and T. V. Ramakrishnan, *Reviews of Modern Physics* **57**, 287.
- [39] W. H. Choi, H. Koh, E. Rotenberg, and H. W. Yeom, *Phys. Rev. B* **75**, 075329 (2007).
- [40] S. Gueron, "QUASIPARTICLES IN a DIFFUSIVE CONDUCTOR: INTERACTION AND PAIRING,".